# Unexpected CO Dependencies, Catalyst Speciation, and Single Turnover Hydrogenolysis Studies of Hydroformylation via High Pressure NMR Spectroscopy

Anna C. Brezny and Clark R. Landis*

Department of Chemistry, University of Wisconsin—Madison, 1101 University Avenue, Madison, Wisconsin 53706, United States

S *Supporting Information*

ABSTRACT: Rhodium bis(diazaphospholane) (BDP) catalyzed hydroformylation of styrene is sensitive to CO concentration, and drastically different kinetic regimes are affected by modest changes in gas pressure. The Wisconsin High Pressure NMR Reactor (WiHP-NMRR) has enabled the observation of changes in catalyst speciation in these different regimes. The apparent discrepancy between catalyst speciation and product distribution led us to report the first direct, noncatalytic quantitative observation of hydrogenolysis of acyl dicarbonyls. Analysis and modeling of these experiments show that not all catalyst is shunted through the off-cycle intermediates and this contributes to the drastic mismatch in selectivities. The data herein highlight the complex kinetics of Rh(BDP) catalyzed hydroformylation. In this case, the complexity arises from competing kinetic and thermodynamic preferences involving formation and isomerization of the acyl mono- and dicarbonyl intermediates and their hydrogenolysis to give aldehydes.
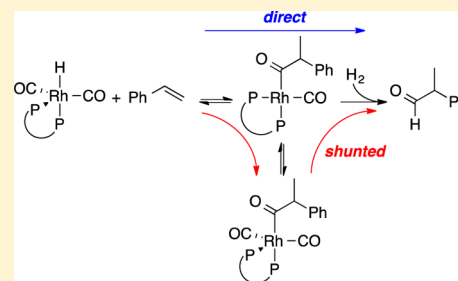
■ INTRODUCTION

Hydroformylation (Scheme 1) is one of the largest scale organotransition metal catalyzed reactions in chemical industry.

Scheme 1. Hydroformylation of Alkenes
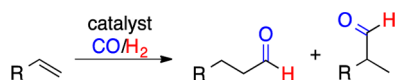
The transformation of an alkene to an aldehyde with 1:1 CO/H$_2$ (syngas) is a one-carbon homologation that adds considerable functionality in a single step.[1]

Although commodity scale applications primarily focus on the linear aldehyde, the chiral, branched aldehydes are attractive precursors for fine-chemical products such as pharmaceuticals.[2] In the last 25 years, there have been great advances in the development of chiral ligands for asymmetric hydroformylation (AHF).[3] A challenge in this reaction is the ability to obtain both high regio- and enantioselectivity while maintaining useful rates. The class of 3,4-bis(diazaphospholane) (BDP) ligands have shown excellent selectivity for a wide range of structurally diverse alkenes with turnover frequencies greater than one per second (Figure 1).[4]

In 1961, Heck and Breslow proposed a mechanism for cobalt-catalyzed hydroformylation that remains generally accepted for rhodium systems (Scheme 2).[5] Although this mechanism outlines the sequence of transformations that constitute the overall reaction, only more detailed kinetic and extra-kinetic analyses can reveal the origins of regioselectivity, enantioselectivity, and rate control. Such analyses include
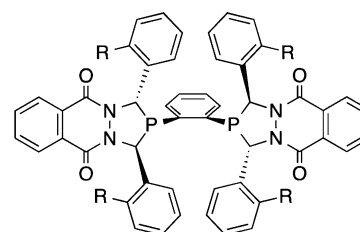

Figure 1. Structure of (*S,S*)-3,4-bis(diazaphospholane) (BDP). This work uses racemic ligand with R = H.

applications of isotopic labels, interception and characterization of catalyst intermediates, *operando* examination of catalyst speciation, and kinetic studies of the catalytic reaction. For example, deuterioformylation studies probe the reversibility of the formation of Rh-alkyls (**4**). With some catalysts and reaction conditions, this step is irreversible, thus indicating that selectivity is fixed at the alkene insertion step.[6]

However, in Rh(BDP)-catalyzed hydroformylation, the alkyl intermediates are known to isomerize for a variety of olefin substrates. Reversible formation of **4** has been demonstrated under catalytic conditions by analysis of product isotope distributions in the presence of D$_2$ and CO. Under noncatalytic conditions, the acyl dicarbonyl isomers (**7**) have been intercepted, characterized, and observed to interconvert.[6j,7] According to the Heck and Breslow mechanism, such interconversion must proceed via alkyl species. In such cases,

Scheme 2. General Mechanism for Hydroformylation
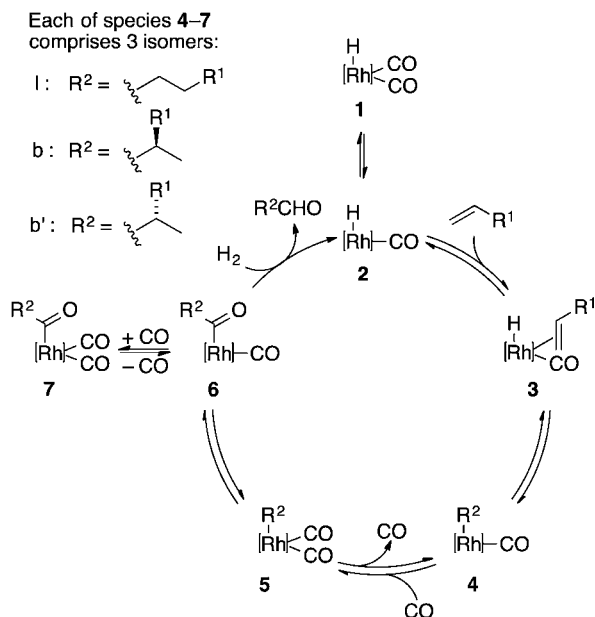
the product selectivity cannot be attributed to the control of a single elementary step.

In many studies of bisphosphine-modified rhodium catalysts for hydroformylation, the rate laws can be classified as type-I or type-II, as coined by van Leeuwen and Claver.[1b] Characteristics of type-I kinetics include a rate law (eq 1) that is independent of [H$_2$], first-order in [catalyst] and [alkene], and inhibited by [CO] and observation of RhH(CO)$_2$(L)$_2$ as the primary resting state. For type-II kinetics, the reaction rate (eq 2) commonly exhibits first-order dependence on [H$_2$] and inhibition by [CO] with catalyst pooling in the form of Rh(acyl)(CO)$_2$(L)$_2$ 7 at high [alkene]. These observations are interpreted to mean that the overall rate is controlled by the rate of hydrogenolysis of 7.

$$\text{Type-I Rate} = \frac{k[\text{cat}][\text{alkene}]}{[\text{CO}]} \tag{1}$$

$$\text{Type-II Rate} = \frac{k[\text{cat}][\text{H}_2]}{[\text{CO}]} \tag{2}$$

Of particular interest to the themes of this manuscript are recent studies of hydroformylation catalysts that feature elegant, quantitative, and simultaneous analysis of catalyst speciation and reaction rates.[8] For example, Vogt's work combined kinetic and *operando* IR spectroscopic studies of the hydroformylation of 3,3-dimethylbut-1-ene as catalyzed by rhodium complexes of monodentate phosphites. They demonstrated that (1) catalyst primarily populates the acyl dicarbonyl 7 with hydrido dicarbonyl 1 appearing in greater concentration as the alkene is consumed; (2) at high alkene concentrations the catalytic reaction obeys type-II kinetics with the rate of aldehyde appearance strictly correlating with the steady-state concentration of acyl dicarbonyl 7; (3) the linear:branched ratio of the acyl dicarbonyl species remained in the range of 1–2:1 over the 298–342 K range while the linear:branched ratio of the aldehyde product remained constant over an individual experiment and ranged from ca. 6–22:1 over a 320–370 K temperature range.[8b,9] These data were interpreted as indicating that hydrogenolysis of the linear acyl dicarbonyl 7 is faster than the branched acyl dicarbonyl and that "the rate-limiting step for both the linear and branched aldehydes was shown to be the hydrogenolysis of the Rh-acyl species."[10]

Selent and co-workers also studied the hydroformylation of 3,3-dimethylbut-1-ene using a different bulky monophosphite ligated rhodium catalyst. This work utilizes a Michaelis–Menten analysis in which "the rate of product formation is limited by the hydrogenolytic step of the mechanism over the entire conversion range."[8c] Garland's examination of the hydroformylation of styrene by an unmodified rhodium catalyst also led to a similar conclusion: "hydrogenolysis of the the two acyl rhodium intermediates represents the rate-limiting step for aldehyde formation."[8a]

However, the observed off-cycle acyls, 7, do not lie on the catalytic cycle, which raises a fundamental question that is general to all catalytic reactions: to what extent is the catalytic rate controlled by conversion of off-cycle species to the product? Because the acyl dicarbonyls are present as both linear and branched isomers, the role of off-cycle species in the control of regioselectivity, also, naturally arises.

Herein we report kinetic studies of the nonasymmetric hydroformylation of styrene as catalyzed by racemic Rh(BDP) complexes. Our report begins with a summary of prior *operando* studies of hydroformylation kinetics and catalyst speciation. We then describe new catalytic results obtained by *operando* NMR using the Wisconsin High Pressure NMR Reactor (WiHP-NMRR) that demonstrate unexpected overall kinetics. The data presentation concludes with kinetic characterization of the noncatalytic hydrogenolysis of linear and branched isomers and the development of a robust kinetic model that describes both catalytic and noncatalytic kinetic data. We finish with an analysis of direct *vs* shunted pathways to product formation that demonstrates the confusion that may result when a catalyst primarily accumulates as off-cycle species.

■ RESULTS AND DISCUSSION

Operando **Spectroscopy and Hydroformylation.** The two most common *operando* methods for study of catalytic hydroformylation are IR and NMR spectroscopy. IR is a natural choice due to the relatively high sensitivity (detection of less than 1 mM concentrations) afforded by the strongly absorbing C−O and M−H stretches, the lower expense of IR spectrometers, and the development of principal component decompositions that enable the extraction of spectra for individual components from complex spectra. Excellent examples of combined kinetic/*operando* IR spectroscopic studies of hydroformylation are provided by recent work of Garland, Selent, and Vogt (*vide supra*).[8,11] NMR methods, while less sensitive and more expensive, bring tools for elucidating detailed structures, simple correlation of peak areas with concentrations, and applicability for cases where IR spectra are crowded or structurally insensitive. The Wisconsin High Pressure NMR Reactor (WiHP-NMRR) enables the observation of reactions under known, constant gas concentration with active gas−liquid mixing and injection of reagents under pressure.[12] Previously, we have shown that key intermediates can be intercepted and rigorously characterized by NMR under low-pressure conditions; these assignments facilitate the interpretation of data collected by *operando* NMR methods.[7]

Operando **Study of the Catalytic Hydroformylation of Styrene as Studied by WiHP-NMRR at 313 K.** In our previous studies of the Rh(BDP)-catalyzed hydroformylation of styrene, several alkyl and acyl on- and off-cycle intermediates
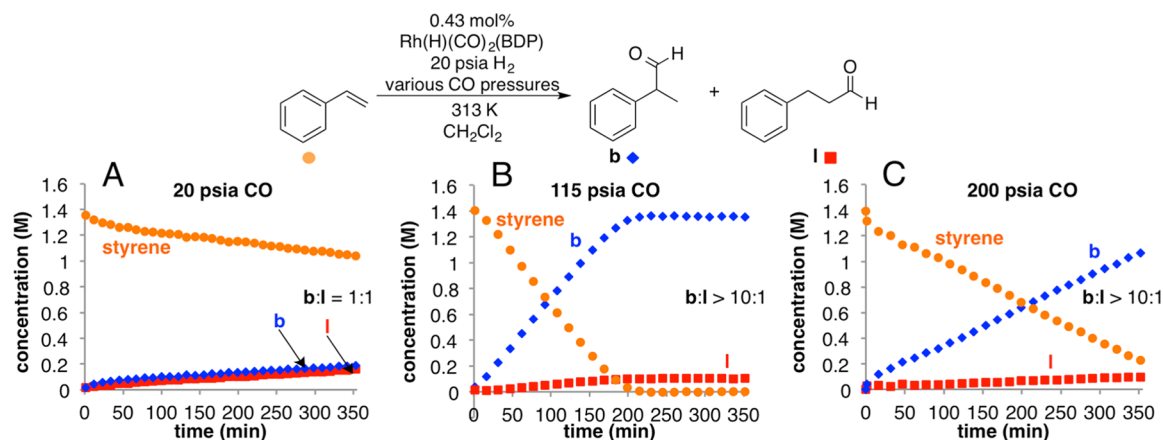
Figure 2. Effect of CO pressure on rates and selectivity in hydroformylation. Time course data were collected using the Wisconsin High Pressure NMR reactor (WiHP-NMRR) (1.4 M styrene, 6 mM Rh(H) (CO)$_2$(BDP), 313 K, 20 psia H$_2$, and varied CO pressures: 20 psia CO (A), 115 psia CO (B), and 200 psia CO (C)).
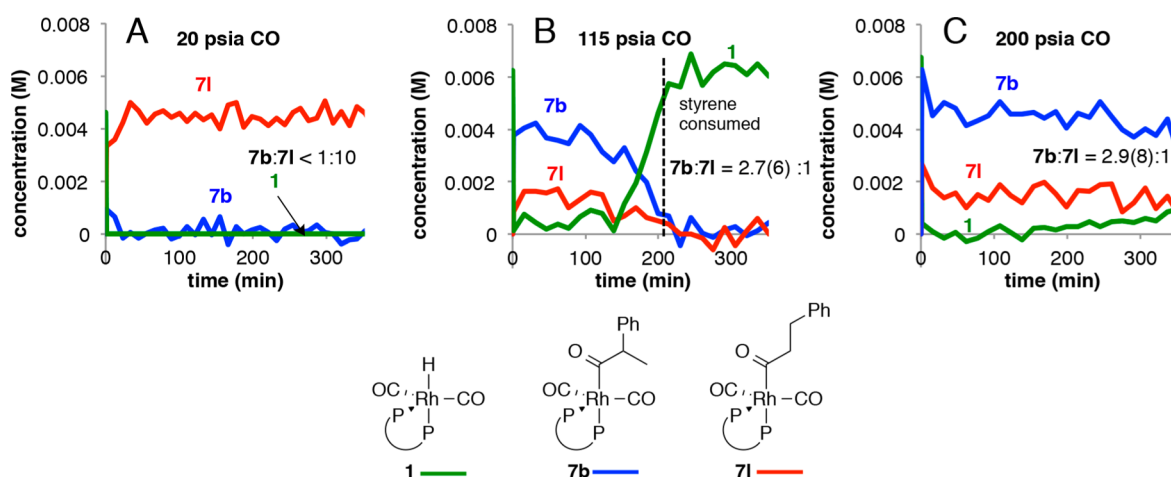

Figure 3. Catalyst speciation observed during hydroformylation reactions in the WiHP-NMRR under the same conditions shown in Figure 2 (1.4 M styrene, 6 mM Rh(H) (CO)$_2$(BDP), 313 K, 20 psia H$_2$, and varied CO pressure: 20 psia CO (A), 115 psia CO (B), and 200 psia CO (C)).

were characterized in the absence of H$_2$ and low CO pressure without active gas−liquid mixing at low temperature.[7a] Formation of the branched acyl dicarbonyl (**7b**) is kinetically favored, but it isomerizes to the thermodynamically preferred linear species (**7l**) under these CO-starved conditions. For quantitative analysis of the kinetic selectivity, see Figure S9. These studies demonstrate intrinsic kinetic and thermodynamic selectivities for acyl formation but do not necessarily apply to catalytic conditions.

Data collected for catalytic hydroformylation by *operando* ^{1}H NMR spectroscopy at 313 K and 20 psia H$_2$ are presented in Figure 2. The data of plots B and C are consistent with type-II kinetics[1b] for which the resting state is an acyl dicarbonyl (**7**) and the reaction rate is dependent on [H$_2$] with inhibition by CO (see the Supporting Information for the dependence of the rate on dihydrogen concentration). Thus, increasing the CO pressure from 115 psia CO to 200 psia results in approximate halving of the reaction rate. However, the changes upon *decreasing* the CO pressure from 115 psia CO to 20 psia are unexpected: a dramatic *decrease* of both the reaction rate *and* regioselectivity is observed. Does the catalyst change resting state over the three different kinetic regimes represented?

The reactions described in Figure 2 use concentrations of catalyst that enable direct observation of catalyst speciation by

^{31}P{^{1}H} NMR spectroscopy. In these experiments, the branched and linear acyl dicarbonyl species are the primary catalyst resting states (Figure 3). Under low CO pressures (20 psia, plot A), rhodium pools primarily as the linear acyl dicarbonyl **7l**, but under higher CO pressures (115 and 200 psia, plots B and C), it sits as a ∼3:1 **7b**:**7l** mixture. These data are consistent with thermodynamic control of the **7b**:**7l** ratio at the lowest CO pressure and kinetically controlled ratios at the two higher pressures. Low CO pressures allow sufficiently rapid interconversion of linear and branched acyls **7** such that an equilibrium distribution is attained. Previous noncatalytic studies established a strong thermodynamic preference for **7l** over **7b**, yielding a 33:1 ratio of **7l**:**7b** at −20 °C. For the catalytic conditions of Figure 2, it is reasonable that higher CO pressures suppress isomerization of the Rh-alkyls **4l** and **4b** because CO trapping of **4**, ultimately to yield **6**, is more efficient. Additionally, isomerization by reversion of the acyl **6** to the alkyl **4** likely is slower at high pressure because such reversion requires CO dissociation. We have conducted deuteroformylation studies at 40 and 80 psia CO, the results of which are consistent with this interpretation: deuterium scrambling, hence alkyl isomerization, is inhibited by increased CO pressure and decreased temperatures (see the Supporting Information). There are three observations that stand out with

the data in Figures 2 and 3: (1) the rate law is not described fully by either type-I or type-II scenarios; (2) different conditions lead to large differences in rate and catalyst speciation; (3) the steady-state ratio of the acyls (**7b**:**7l**) does not equal the ratio of aldehyde products (**b**:**l**).

The difference in overall rates between the reactions at 115 and 200 psia CO is most simply attributed to CO inhibition, consistent with type-II kinetics. The common interpretation is that acyl dicarbonyl species (**7**) or hydrido dicarbonyl (**1**) must lose one ligand to re-enter the cycle; thus, at higher pressures of CO, the rate is slower.

The dramatic differences in rate between the low CO pressure (20 psia, Figure 2A) versus the higher pressure reactions (115 or 200 psia, Figure 2B,C) clearly correlate with changes in the catalyst resting state. Interestingly, at low (20 psia) CO pressures, the ratio **7l**:**7b** is ~20:1 but yields a 1:1 **b**:**l** ratio of product aldehydes. *Only at low CO pressures* do the catalytic data of Figures 2 and 3 superficially appear to correspond to Curtin−Hammett kinetics for which there is rapid isomerization between the acyl dicarbonyls (**7**), and the rates of product formation are described by eqs 3 and 4 (Figure 4).

$$\frac{d[b]}{dt} = k_b[\mathbf{7b}] \tag{3}$$

$$\frac{d[l]}{dt} = k_l[\mathbf{7l}] \tag{4}$$
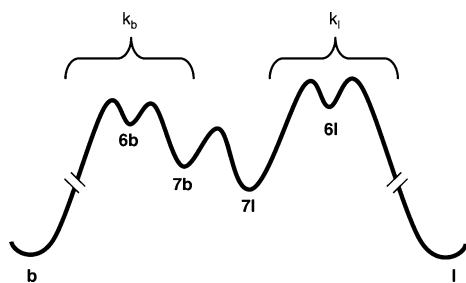

Figure 4. Curtin−Hammett free energy scheme that may describe catalytic data in low [CO] regimes.

In order to explain the 1:1 ratio of linear and branched aldehyde products, **7b** must undergo faster hydrogenolysis than **7l**.[13] Strictly speaking, at the higher pressures of Figures 2B,C and 3B,C, Curtin−Hammett behavior does not explain the regioselectivity because **7b** and **7l** are not in equilibrium. Regardless of whether or not the acyls are in equilibrium, eqs 3 and 4 can still be true under conditions of turnover-limiting hydrogenolysis.

Direct Measurement of the Kinetics of Hydrogenolysis of Acyl Dicarbonyls at 290 K. In Vogt's analysis of hydroformylation,[8b] the appearance of branched and linear products was modeled by eqs 3 and 4. The steady state concentrations of **7b** and **7l** were determined by direct *operando* observation; the apparent rate constants k_b and k_l depend on [CO] and [H$_2$]. In order to evaluate the role of off-cycle species **7b** and **7l** in determining the reaction kinetics and selectivity, it is useful to know their intrinsic rates of hydrogenolysis. Therefore, we devised single turnover experiments that directly measure these rates.

In the WiHP-NMRR, a 1:1 mixture of **7b** and **7l** was formed in the absence of hydrogen by allowing 1 equiv of styrene to react with hydride **1** at 310 K and 18 psia of CO. When the **7b**:**7l** ratio reached approximately 1:1, the reaction was cooled to 290 K and additional CO and H$_2$ were added to the reactor with active gas−liquid mixing. Under these conditions, the acyls produce the aldehyde products without any further interconversion of acyl dicarbonyls; i.e., the initial concentrations of **7b** + **7b'** and **7l** correspond to the final concentrations of branched and linear aldehydes, respectively (Figure 5). We note that the minor branched diastereomer **7b'** is barely visible under these conditions and is ignored in our subsequent analysis. Temperatures lower than those of the catalytic experiments of Figures 2 and 3 are necessary to slow the rate of hydrogenolysis for convenient monitoring by ^{1}H and ^{31}P NMR spectroscopies. Data were collected under three CO pressures (18, 35, and 70 psia CO) and a wide range of H$_2$ pressures ranging from 20 to 530 psia. As expected, on the basis of the rate laws assuming a steady state approximation on **6** (eqs 5−10), the pressure of hydrogen enhances the rate of hydrogenolysis, and CO inhibits the reaction. These data
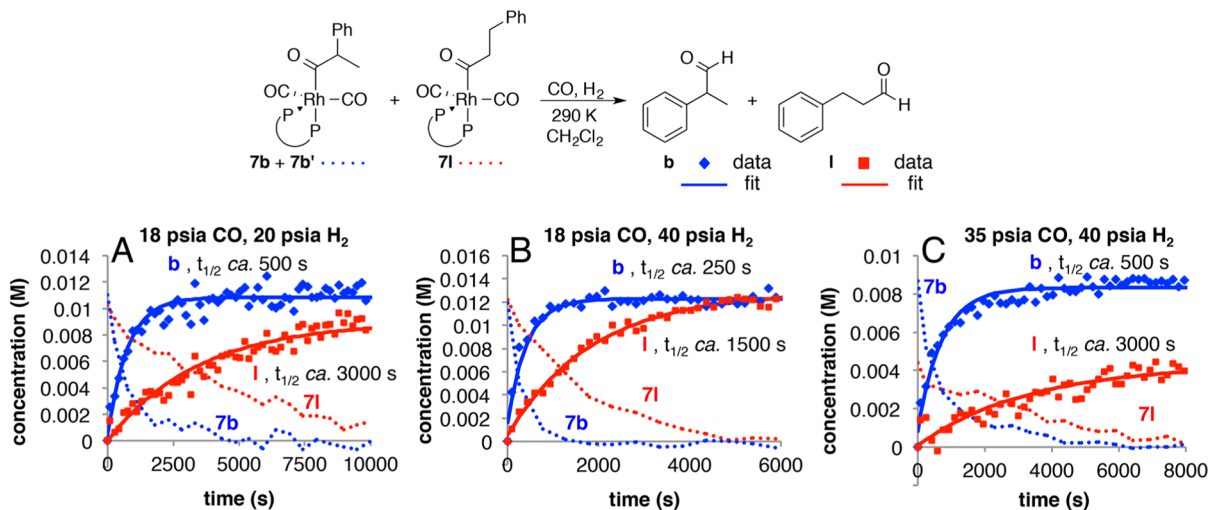

Figure 5. Single turnover experiments in the WiHP-NMRR. The branched acyl dicarbonyl undergoes hydrogenolysis faster than the linear isomer (CO loss and/or reaction with H$_2$) (~22 mM Rh(BDP) as 1:1 mixture of acyls, 290 K, varied CO and H$_2$ pressures: 18 psi CO, 20 psi H$_2$ (A); 18 psi CO, 40 psi H$_2$ (B); 35 psi CO, 40 psi H$_2$ (C)). The points indicate the experimental data, and solid lines represent the modeled fits.

corroborate the hypothesis that **7b** undergoes hydrogenolysis faster than **7l**.

$$[\mathbf{6b}] = \frac{k_{1b}[\mathbf{7b}]}{k_{2b}[H_2] + k_{-1b}[CO]} \quad (5)$$

$$\frac{d[\mathbf{b}]}{dt} = k_{2b}[\mathbf{6b}][H_2] \quad (6)$$

$$\frac{d[\mathbf{b}]}{dt} = \frac{k_{2b}k_{1b}[\mathbf{7b}][H_2]}{k_{2b}[H_2] + k_{-1b}[CO]} \quad (7)$$

$$[\mathbf{6l}] = \frac{k_{1l}[\mathbf{7l}]}{k_{2l}[H_2] + k_{-1l}[CO]} \quad (8)$$

$$\frac{d[\mathbf{l}]}{dt} = k_{2l}[\mathbf{6l}][H_2] \quad (9)$$

$$\frac{d[\mathbf{l}]}{dt} = \frac{k_{2l}k_{1l}[\mathbf{7l}][H_2]}{k_{2l}[H_2] + k_{-1l}[CO]} \quad (10)$$

The data show that increasing pressures of H_2 affect saturation of the rate of hydrogenolysis. Such saturation indicates efficient competitive trapping of **6** by dihydrogen vs reassociation of CO. In this limit, the rate of hydrogenolysis is controlled by the rate of CO dissociation from **7** (k_{1b} and k_{1l}, see Figure 6). Global modeling of all the empirical kinetic data
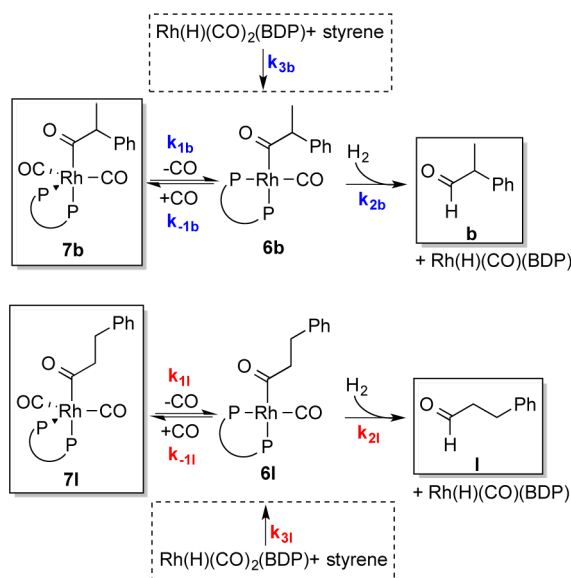

Figure 6. Kinetic model for hydrogenolysis of acyl dicarbonyl complexes **7b** and **7l**. Species indicated with solid boxes are directly observable by NMR spectroscopy; reactions indicated with dashed boxes are only relevant to catalytic reactions.

for the single turnover hydrogenolysis experiments with the program COPASI,[14] in accordance with the kinetic model represented by eqs 5–10, led to values for the rate constants k_{1b}, k_{1l}, k_{-1b}/k_{2b}, and k_{-1l}/k_{2l} (Table 1). Because the acyl monocarbonyl species (**6b** and **6l**) are not observed by NMR, the ratios k_{-1b}/k_{2b} and k_{-1l}/k_{2l} can be determined — not the values of the individual rate constants. Representative modeled fits are shown in Figure 5; for all modeled data, see the Supporting Information.

Table 1. Computed Rate Constants for Hydrogenolysis of Acyl Dicarbonyl Complexes

	value	standard deviation
k_{1b}	2.3×10^{-2} (s^{-1})	1×10^{-3}
k_{1l}	6.4×10^{-3} (s^{-1})	5×10^{-4}
k_{-1b}/k_{2b}	8.2	0.2
k_{-1l}/k_{2l}	10.5	0.3

These data quantitatively show that CO loss from the branched acyl dicarbonyl is approximately 4-fold faster than that from the linear isomer. At equal concentrations of H_2 and CO, the branched acyl monocarbonyl (**6b**) is just 8 times more likely to be trapped by CO than react with dihydrogen; the linear acyl monocarbonyl (**6l**) is 10 times more likely to be trapped by CO. These data indicate just modest differences (factors of 4−5) in the hydrogenolysis rates of **7b** and **7l**. Application of these rates to catalytic data at 313 K cannot account for the mismatch between steady-state acyl concentrations and the aldehyde product distributions. In order to draw quantitative conclusions and because the rates of the single turnover experiments are too fast at 313 K, we chose to examine catalytic data at 290 K.

WiHP-NMRR Catalytic Hydroformylation at 290 K. In order to compare the rates of noncatalytic hydrogenolysis with catalytic rates, *operando* NMR studies of the catalytic reaction were performed. Both the catalyst speciation and the rates of linear and branched aldehyde were followed over a range of CO and H_2 pressures (20 or 200 psia of each gas) (Figure 7). The catalytic data at 290 K were successfully modeled using the kinetic model of Figure 6 and the rate constants obtained from single-turnover hydrogenolysis experiments. For this simplified model, the reactions of **1** and styrene to form **6b** and **6l** are represented as irreversible pseudoelementary steps. Because the effect of [CO] on these pseudoelementary steps is not known, the phenomenological rate constants, k_{3b} and k_{3l}, for these steps were fitted for each set of catalytic reaction conditions. The results are shown in Table 2 and Figure 7. Consistent with CO inhibition, the apparent rate constants for acyl formation ($k_{3b/l}$) are inversely proportional to CO pressure; i.e., increasing the CO pressure from 20 to 200 psia decreases the rate constant by an order of magnitude. These rate constants are approximately independent of [H_2].

Interpretation of the Difference in Catalytic Kinetics at 313 and 290 K. In Figure 2, catalytic data at 313 K show large and complex changes in selectivity and rate upon changing the CO pressure. In contrast, the data at 290 K (Figure 7) exhibit much smaller effects; for the CO pressure ranges explored, the product selectivity remains almost constant. As discussed above, deuteroformylation experiments show greater H/D scrambling at higher temperatures and lower CO pressures (see the Supporting Information). Therefore, the reactions at higher temperature (313 K) and low CO pressure (20 psia) allow for greater isomerization of the catalyst to the thermodynamically favored acyl dicarbonyl but an overall slower linear pathway. The result is low regioselectivity (b:1 = 1:1) and slow product formation. At higher CO pressures (115 or 200 psia), the isomerization is slowed such that the majority of the catalyst remains on the faster, branched pathway. In contrast, at 290 K, even at the low CO pressures, the isomerization of alkyls is slow enough such that the product distribution is relatively unaffected and the rates display the expected CO inhibition.
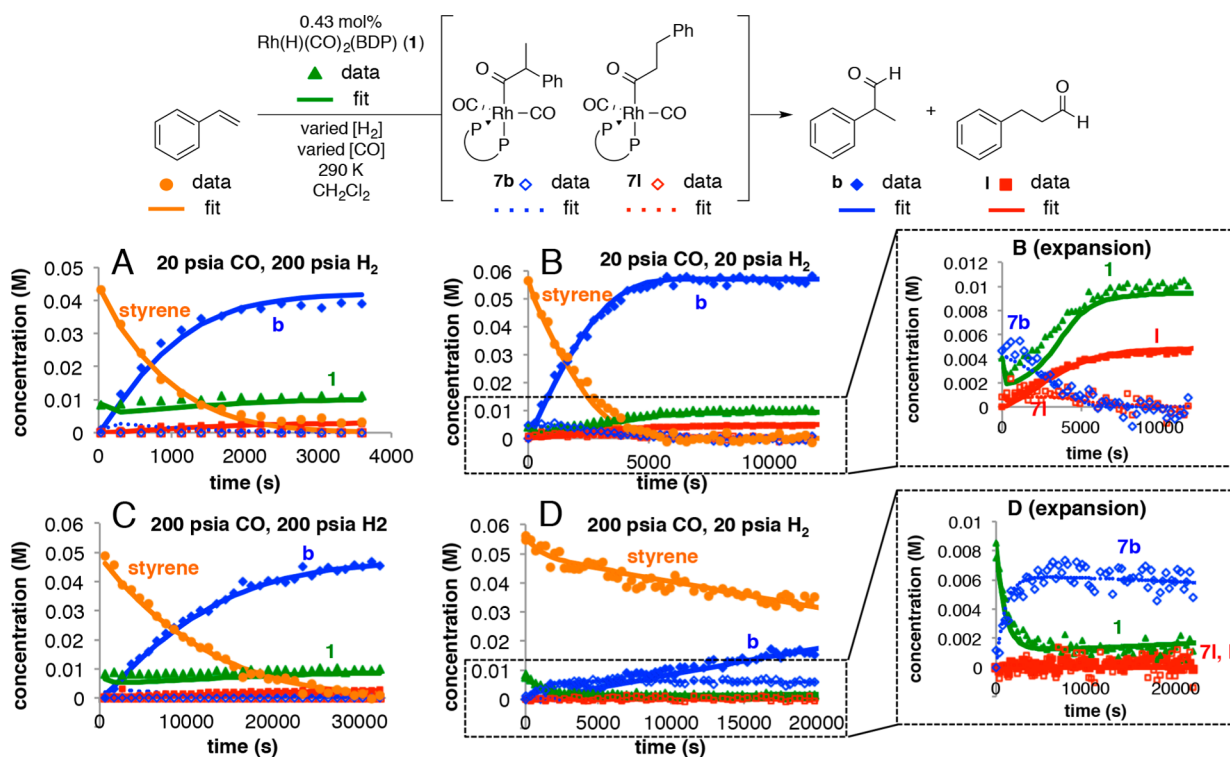
Figure 7. Time courses for hydroformylation of styrene collected in the WiHP-NMRR at 290 K (0.06 M styrene, 0.01 M Rh(H) (CO)$_2$(BDP), 290 K, and varied gas pressures: 20 psia CO, 200 psia H$_2$ (A), 20 psia CO, 20 psia H$_2$ (B), 200 psia CO, 200 psia H$_2$ (C), 200 psia CO, 20 psia H$_2$ (D)). Experimental data shown as points; modeled fits displayed as lines. Plots B and D show expansions for clarity of low concentration species.

Table 2. Computed Rate Constants (k_{3b}, k_{3l}, See Figure 6) for Formation of Acyl Monocarbonyl Complexes

P_{CO}	P_{H_2}	k_{3b} value (M^{-1} s^{-1})	standard deviation	k_{3l} value (M^{-1} s^{-1})	standard deviation
20	20	0.110	0.003	0.0070	0.0003
200	20	0.0151	0.0003	0.00061	0.00005
20	200	0.122	0.005	0.0083	0.0006
200	200	0.0113	0.0002	0.00066	0.00003

Does the Observed Catalytic Rate Correspond to Rate-Limiting Hydrogenolysis of the Acyl Dicarbonyls? Comparison of the noncatalytic hydrogenolysis rate (using the steady-state concentrations of $[7b]_{ss}$ = 4.8(5) mM and $[7l]_{ss}$ = 1.36(6) mM seen over the first 50% conversion in catalytic experiments) with the catalytic rate over the first 50% conversion conclusively demonstrates that the catalytic rate is *faster* than hydrogenolysis. For example, at 20 psia CO and 20 psia H$_2$, the catalytic rates for making linear and branched products are 8.3(1) × 10^{-7} and 1.8(1) × 10^{-5} M s^{-1}, respectively, whereas the hydrogenolysis rates are computed to be 3.6(3) × 10^{-7} and 5.2(6) × 10^{-6} M s^{-1}, respectively.[15] In other words, the hydrogenolysis rates are just 44(4) and 29(4)% of the catalytic rates for branched and linear products, respectively. We conclude that the catalytic rates are not controlled solely by the hydrogenolysis of **7**.

If the catalyst pools in the form of the acyl dicarbonyls **7b** and **7l** and the observed rate law is independent of [alkene], first order in [H$_2$], and inhibited by CO, why is the rate not predicted by a model of rate-limiting hydrogenolysis? Although intermediates **6b** and **6l** precede product formation in both catalytic hydroformylation and noncatalytic, single turnover hydrogenolysis experiments, steady-state concentrations of

these intermediates differ in catalytic and noncatalytic experiments. Under the single-turnover conditions, **6** can only be formed by dissociation of CO from the acyl dicarbonyl (**7**). In contrast, under catalytic conditions, **6** can also be formed directly from the alkyl **4**. Thus, there is a more efficient pathway to aldehyde in which the catalyst goes directly from **6** to aldehyde product without being diverted off-cycle to **7**. Applying the steady state approximation to [**6**], the concentrations and rate laws in eqs 11–14 result for the model depicted in Figure 8. This kinetic model represents the CO association and insertion steps that convert the alkyl monocarbonyl (**4**) to the acyl monocarbonyl (**6**) as a single pseudoelementary step with the composite rate constant k_4. The reaction of **2** and styrene to give the alkyl (**4**) is
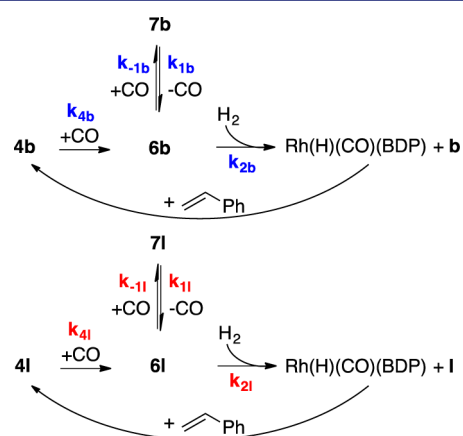

Figure 8. Simplified model for catalytic hydroformylations highlighting the importance of [alkyl] (**4**) in the rate of formation of aldehyde.

represented without a rate constant because it is presumed to be fast by the zeroth order dependence on styrene and no observation of **2** during catalysis. The forms of the catalytic rate law demonstrate that the rates of linear and branched aldehyde formation under catalytic conditions are (a) controlled by the steady-state concentrations of **6l** and **6b**, respectively (eqs 12 and 14), and (b) the steady-state concentrations of **6** are greater under catalytic than noncatalytic conditions (eqs 11 and 13). Indeed, relative to the single turnover conditions, the catalytic steady-state concentration of **6b** increases more than that of **6l**. This differential increase occurs because formation of the branched alkyl **4b** is kinetically preferred over the linear alkyl **4b**, as conclusively demonstrated by our previous studies.[7a]

$$[\mathbf{6b}] = \frac{k_{1b}[\mathbf{7b}] + k_{4b}[\mathbf{4b}][CO]}{k_{2b}[H_2] + k_{-1b}[CO]} \tag{11}$$

$$\frac{d[\mathbf{b}]}{dt} = \frac{(k_{1b}[\mathbf{7b}] + k_{4b}[\mathbf{4b}][CO])k_{2b}[H_2]}{k_{2b}[H_2] + k_{-1b}[CO]} \tag{12}$$

$$[\mathbf{6l}] = \frac{k_{1l}[\mathbf{7l}] + k_{4l}[\mathbf{4l}][CO]}{k_{2l}[H_2] + k_{-1l}[CO]} \tag{13}$$

$$\frac{d[\mathbf{l}]}{dt} = \frac{(k_{1l}[\mathbf{7l}] + k_{4l}[\mathbf{4l}][CO])k_{2l}[H_2]}{k_{2l}[H_2] + k_{-1l}[CO]} \tag{14}$$

The analysis above describes scenarios that apply to *any* catalytic reaction with off-cycle species. The most efficient catalysis occurs for the scenario whereby all of the catalytic species are on-cycle. Any distribution of catalyst off-cycle, or even to the slower of concurrent cycles, must decrease the catalytic rate. As catalyst and substrate circuit the catalytic cycle, there are junctions where the catalyst temporarily may go off-cycle (e.g., intermediates **2** and **6**). We refer to these as "shunted" pathways to product, in opposition to the "direct" pathway for which the catalyst remains on-cycle. The direct pathway may contribute substantially to the overall rate even under conditions in which the only *detectable* catalyst is off-cycle. For the hydroformylation catalysts and conditions examined here, even though all detectable catalyst species lie off-cycle (as **7l**, **7b**, and **1**) and the catalytic rate law *appears* to indicate rate-limiting hydrogenolysis, detailed analysis reveals that the majority of products (55% of the linear and 70% of the branched aldehydes) originate from direct, on-cycle pathways. These percentages vary with reaction conditions. For example, the reaction at 200 psia CO (Figure 7D) using the same analysis reveals that only 20% of the branched acyl monocarbonyl reacts directly while 80% is shunted off-cycle.

The hydroformylation data presented herein demonstrate that it is inappropriate to identify the reaction as rate-limited by the hydrogenolysis of acyl dicarbonyls. Such dissection of the rates into "direct" and "shunted" components could be made only because elementary steps of the full catalytic reaction could be characterized independently.

The analysis given above directly relates to "Halpern's rules" which cast doubt on the role of observable catalyst-derived species under catalytic conditions: species sufficiently stable to accumulate are likely to lie off-cycle. For the example of Rh(BDP)-catalyzed hydroformylation under the conditions reported above, many of the alkene molecules are transformed to aldehyde without ever existing as the off-cycle **7**, even though the acyl dicarbonyls are the primary observed catalyst species.

CONCLUSIONS

Operando observation of hydroformylation by WiHP-NMRR reveals complex kinetics and an apparent mismatch between the b:l ratio of the acyl resting states and the product distribution. This discrepancy led us to study the rates of hydrogenolysis of branched and linear acyls via single turnover experiments. Although the branched acyl dicarbonyl (**7b**) undergoes faster hydrogenolysis than the linear isomer (**7l**), these differences in rates cannot fully explain the observed catalytic behavior. Detailed analysis distinguishes between direct and shunted pathways to product. Shunted pathways are those in which intermediates go off-cycle prior to forming product. Even under conditions where all of the detectable catalyst lies off-cycle, this analysis at 290 K reveals that 70% of the branched product and 55% of the linear product form by the direct pathway, bypassing **7b** and **7l**. These differences in catalytic activity are consistent with our observation of higher **7l** concentrations relative to **7b** than are observed in the final product distribution; these mismatches are more prevalent at higher reaction temperatures.

These results highlight the complex mechanism of the hydroformylation reaction and the value of *operando* NMR studies of both single-turnover and catalytic kinetics for a prototypical hydroformylation reaction. More generally, the results provide a quantitative illustration for why superficially labeling a step as selectivity-determining, rate-limiting, rate-controlling, or turnover-limiting can be problematic, especially when only the apparent catalytic rate law is known without knowledge of rates and rate laws for individual steps nor the speciation of catalyst under a variety of conditions. These issues apply to any and all catalytic reactions.

ASSOCIATED CONTENT

Ⓢ Supporting Information
The Supporting Information is available free of charge on the ACS Publications website at DOI: 10.1021/jacs.6b12533.

Experimental procedures, plots, and modeling data (PDF)

AUTHOR INFORMATION

Corresponding Author
*landis@chem.wisc.edu
ORCID ⓘ
Clark R. Landis: 0000-0002-1499-4697
Notes
The authors declare no competing financial interest.

ACKNOWLEDGMENTS

REFERENCES

(1) For reviews of hydroformylation, see: (a) Agbossou, F.; Carpentier, J.-F.; Mortreux, A. *Chem. Rev.* **1995**, *95*, 2485−2506. (b) van Leeuwen, P. W. N. M.; Claver, C. *Rhodium Catalyzed Hydroformylation*; Kluwer Academic Publishers: Dordrecht, The Netherlands, 2000. (c) Wiese, K.-D.; Obst, D. *Top. Organomet. Chem.* **2006**, *18*, 1−33. (d) Franke, R.; Selent, D.; Börner, A. *Chem. Rev.* **2012**, *112*, 5675−5732.

(2) Botteghi, C.; Paganelli, S.; Schionato, A.; Marchetti, M. *Chirality* **1991**, *3*, 355−369.

(3) For examples of catalysts for asymmetric hydroformylation, see: (a) Wink, D. J.; Kwok, T. J.; Yee, A. *Inorg. Chem.* **1990**, *29*, 5006−5008. (b) Gladiali, S.; Pinna, L. *Tetrahedron: Asymmetry* **1991**, *2*, 623−632. (c) Sakai, N.; Nozaki, K.; Mashima, K.; Takaya, H. *Tetrahedron: Asymmetry* **1992**, *3*, 583−586. (d) Sakai, N.; Mano, S.; Nozaki, K.; Takaya, H. *J. Am. Chem. Soc.* **1993**, *115*, 7033−7034. (e) Babin, J. E.; Whiteker, G. T. Asymmetric syntheses, World Patent, WO1993003839, 1993. (f) Sakai, N.; Nozaki, K.; Takaya, H. *J. Chem. Soc., Chem. Commun.* **1994**, 395−396. (g) Nanno, T.; Sakai, N.; Nozaki, K.; Takaya, H. *Tetrahedron: Asymmetry* **1995**, *6*, 2583−2591. (h) Masdeu-Bultó, A. M.; Orejón, A.; Castellanos, A.; Castillón, S.; Claver, C. *Tetrahedron: Asymmetry* **1996**, *7*, 1829−1834. (i) Nozaki, K.; Sakai, N.; Nanno, T.; Higashijima, T.; Mano, S.; Horiuchi, T.; Takaya, H. *J. Am. Chem. Soc.* **1997**, *119*, 4413−4423. (j) Nozaki, K.; Li, W.-g.; Horiuchi, T.; Takaya, H. *Tetrahedron Lett.* **1997**, *38*, 4611−4614. (k) Horiuchi, T.; Ohta, T.; Shirakawa, E.; Nozaki, K.; Takaya, H. *J. Org. Chem.* **1997**, *62*, 4285−4292. (l) Breeden, S.; Cole-Hamilton, D. J.; Foster, D. F.; Schwarz, G. J.; Wills, M. *Angew. Chem., Int. Ed.* **2000**, *39*, 4106−4108. (m) Cobley, C. J.; Gardner, K.; Klosin, J.; Praquin, C.; Hill, C.; Whiteker, G. T.; Zanotti-Gerosa, A.; Petersen, J. L.; Abboud, K. A. *J. Org. Chem.* **2004**, *69*, 4031−4040. (n) Castillon, S.; Claver, C.; Diaz, Y. *Chem. Soc. Rev.* **2005**, *34*, 702−713. (o) Yan, Y.; Zhang, X. *J. Am. Chem. Soc.* **2006**, *128*, 7198−7202. (p) Rubio, M.; Suárez, A.; Álvarez, E.; Bianchini, C.; Oberhauser, W.; Peruzzini, M.; Pizzano, A. *Organometallics* **2007**, *26*, 6428−6436. (q) Zhang, X.; Cao, B.; Yan, Y.; Yu, S.; Ji, B.; Zhang, X. *Chem. - Eur. J.* **2010**, *16*, 871−877. (r) Gual, A.; Godard, C.; Castillón, S.; Claver, C. *Adv. Synth. Catal.* **2010**, *352*, 463−477. (s) Chikkali, S. H.; Bellini, R.; Berthon-Gelloz, G.; van der Vlugt, J. I.; de Bruin, B.; Reek, J. N. H. *Chem. Commun.* **2010**, *46*, 1244−1246. (t) Robert, T.; Abiri, Z.; Wassenaar, J.; Sandee, A. J.; Romanski, S.; Neudörfl, J.-M.; Schmalz, H.-G.; Reek, J. N. H. *Organometallics* **2010**, *29*, 478−483. (u) Wassenaar, J.; de Bruin, B.; Reek, J. N. H. *Organometallics* **2010**, *29*, 2767−2776. (v) Wang, X.; Buchwald, S. L. *J. Am. Chem. Soc.* **2011**, *133*, 19080−19083. (w) Clarke, M. Ligands for selective asymmetric hydroformylation, World Patent, WO2012016147, 2012. (x) Noonan, G. M.; Fuentes, J. A.; Cobley, C. J.; Clarke, M. L. *Angew. Chem., Int. Ed.* **2012**, *51*, 2477−2480. (y) Chikkali, S. H.; Bellini, R.; de Bruin, B.; van der Vlugt, J. I.; Reek, J. N. H. *J. Am. Chem. Soc.* **2012**, *134*, 6607−6616. (z) Noonan, G. M.; Cobley, C. J.; Mahoney, T.; Clarke, M. L. *Chem. Commun.* **2014**, *50*, 1475−1477. (aa) Fernández-Pérez, H.; Benet-Buchholz, J.; Vidal-Ferran, A. *Chem. - Eur. J.* **2014**, *20*, 15375−15384. (ab) Allmendinger, S.; Kinuta, H.; Breit, B. *Adv. Synth. Catal.* **2015**, *357*, 41−45. (ac) Schmitz, C.; Holthusen, K.; Leitner, W.; Franciò, G. *ACS Catal.* **2016**, *6*, 1584−1589.

(4) (a) Clark, T. P.; Landis, C. R.; Freed, S. L.; Klosin, J.; Abboud, K. A. *J. Am. Chem. Soc.* **2005**, *127*, 5040−5042. (b) Klosin, J.; Landis, C. R. *Acc. Chem. Res.* **2007**, *40*, 1251−1259. (c) Watkins, A. L.; Hashiguchi, B. G.; Landis, C. R. *Org. Lett.* **2008**, *10*, 4553−4556. (d) McDonald, R. I.; Wong, G. W.; Neupane, R. P.; Stahl, S. S.; Landis, C. R. *J. Am. Chem. Soc.* **2010**, *132*, 14027−14029. (e) Watkins, A. L.; Landis, C. R. *Org. Lett.* **2011**, *13*, 164−167. (f) Adint, T. T.; Wong, G. W.; Landis, C. R. *J. Org. Chem.* **2013**, *78*, 4231−4238.

(5) Heck, R. F.; Breslow, D. S. *J. Am. Chem. Soc.* **1961**, *83*, 4023−4027.

(6) (a) Lazzaroni, R.; Uccello-Barretta, G.; Benetti, M. *Organometallics* **1989**, *8*, 2323−2327. (b) Raffaelli, A.; Pucci, S.; Settambolo, R.; Uccello-Barretta, G.; Lazzaroni, R. *Organometallics* **1991**, *10*, 3892−3898. (c) Uccello-Barretta, G.; Lazzaroni, R.; Settambolo, R.; Salvadori, P. *J. Organomet. Chem.* **1991**, *417*, 111−119. (d) Lazzaroni, R.; Settambolo, R.; Uccello-Barretta, G. *Organometallics* **1995**, *14*, 4644−4650. (e) Casey, C. P.; Petrovich, L. M. *J. Am. Chem. Soc.* **1995**, *117*, 6007−6014. (f) Lazzaroni, R.; Uccello-Barretta, G.; Scamuzzi, S.; Settambolo, R.; Caiazzo, A. *Organometallics* **1996**, *15*, 4657−4659. (g) Horiuchi, T.; Shirakawa, E.; Nozaki, K.; Takaya, H. *Organometallics* **1997**, *16*, 2981−2986. (h) Lazzaroni, R.; Settambolo, R.; Uccello-Barretta, G.; Caiazzo, A.; Scamuzzi, S. *J. Mol. Catal. A: Chem.* **1999**, *143*, 123−130. (i) van der Slot, S. C.; Duran, J.; Luten, J.; Kamer, P. C. J.; van Leeuwen, P. W. N. M. *Organometallics* **2002**, *21*, 3873−3883. (j) Watkins, A. L.; Landis, C. R. *J. Am. Chem. Soc.* **2010**, *132*, 10306−10317.

(7) (a) Nelsen, E. R.; Landis, C. R. *J. Am. Chem. Soc.* **2013**, *135*, 9636−9639. (b) Nelsen, E. R.; Brezny, A. C.; Landis, C. R. *J. Am. Chem. Soc.* **2015**, *137*, 14208−14219.

(8) (a) Feng, J.; Garland, M. *Organometallics* **1999**, *18*, 417−427. (b) Güven, S.; Nieuwenhuizen, M. M. L.; Hamers, B.; Franke, R.; Priske, M.; Becker, M.; Vogt, D. *ChemCatChem* **2014**, *6*, 603−610. (c) Kubis, C.; Selent, D.; Sawall, M.; Ludwig, R.; Neymeyr, K.; Baumann, W.; Franke, R.; Borner, A. *Chem. - Eur. J.* **2012**, *18*, 8780−8794.

(9) Raw laws: $d[b]/dt = (k_{6b→1}[7b][H_2])/(K_{6b→7b}[CO])$; $d[l]/dt = (k_{6l→1}[7l][H_2])/(K_{6l→7b}[CO])$. In situ high-pressure IR spectroscopy experimental conditions: $T = 298−343$ K, [3,3-dimethyl-1-butene] = 0.54 M, [Rh] = $3.14 × 10^{−4}$ M, L/Rh = 26, $P_{CO} = 29.75−35.15$ bar, $P_{H_2} = 3.75−6.59$ bar. Deuteroformylation experimental conditions: $T = 323−373$ K, [3,3-dimethyl-1-butene] = 2.7 M, [Rh] = $1.0 × 10^{−4}$ M, L/Rh = 27, $P_{CO} = 20$ bar, $P_{D_2} = 20$ bar. Semibatch experimental conditions: $T = 334−363$ K, [3,3-dimethyl-1-butene] = 1.25−2.93 M, [Rh] = $0.59 × 10^{−4}$ to $2.95 × 10^{−4}$ M, L/Rh = 15−30, $P_{CO} = 9−35.9$ bar, $P_{H_2} = 20−42$ bar.

(10) The term hydrogenolyis does not strictly refer to the reaction of **6** with H₂, only; rapid equilibration of **7** and **6** is assumed such that one could equivalently describe hydrogenolysis of **7** as rate-determining where hydrogenolysis is a composite two-step process.

(11) (a) Kubis, C.; Baumann, W.; Barsch, E.; Selent, D.; Sawall, M.; Ludwig, R.; Neymeyr, K.; Hess, D.; Franke, R.; Börner, A. *ACS Catal.* **2014**, *4*, 2097−2108. (b) Kubis, C.; Sawall, M.; Block, A.; Neymeyr, K.; Ludwig, R.; Borner, A.; Selent, D. *Chem. - Eur. J.* **2014**, *20*, 11921−11931. (c) Kubis, C.; Ludwig, R.; Sawall, M.; Neymeyr, K.; Börner, A.; Wiese, K.-D.; Hess, D.; Franke, R.; Selent, D. *ChemCatChem* **2010**, *2*, 287−295.

(12) Beach, N. J.; Knapp, S. M. M.; Landis, C. R. *Rev. Sci. Instrum.* **2015**, *86*, 104101−104109.

(13) We refer to hydrogenolysis as the overall reaction from resting state **7** to aldehyde; it includes the (reversible) loss of CO and the irreversible reaction with hydrogen to form aldehyde.

(14) Hoops, S.; Sahle, S.; Gauges, R.; Lee, C.; Pahle, J.; Simus, N.; Singhal, M.; Xu, L.; Mendes, P.; Kummer, U. *Bioinformatics* **2006**, *22*, 3067−3074.

(15) The errors for the predicted rate constants were calculated by propagation from the rate constants and the estimated [**7b**] and [**7l**] at the steady state. In the range from 0 to 2000 s, the concentrations of the acyl dicarbonyls remain constant: [**7b**] = 4.8(5) mM and [**7l**] = 1.36(6) mM. The observed rate constants and associated errors were obtained from the experimental data in the same linear region.